Materials Advances

ROYAL SOCIETY OF CHEMISTRY

PAPER

View Article Online
View Journal

Cite this: DOI: 10.1039/d6ma00175k

Design and characterization of a bioinspired green lipoic acid–syringic acid-based hydrogel for wound healing

Navneet Thakur,[ab] Ruchika,[ab] Neha Rana,[ab] Vikram Patial[ab] and Ankit Saneja *[ab]

In this study, we have developed a green hydrogel composed of α-lipoic acid (LA) and syringic acid (SA) for wound healing applications. LA, known for its antioxidant properties, was polymerized through thermally initiated ring-opening polymerization (ROP) to form a poly-LA hydrogel, while SA was incorporated to enhance adhesion and bioactivity. The optimal hydrogel formulation (LA : SA 1 : 0.1) exhibited improved adhesivity and gelation, as confirmed by rheological analysis. Comprehensive characterization using nuclear magnetic resonance spectroscopy (NMR), X-ray diffraction (XRD), X-ray photoelectron spectroscopy (XPS), and scanning electron microscope (SEM) verified the successful cross-linking, amorphous nature, and interconnected morphology of the hydrogel. The functional assays demonstrated that the poly-LA–SA hydrogel (LAS-G) exhibits higher antioxidant activity, as evidenced by DPPH (92.33%) and ABTS (70.92%) radical-scavenging, as well as a significant antibacterial effect against *Staphylococcus aureus* and *Escherichia coli*, compared to the native poly-LA hydrogel (LA-G). *In vivo* studies in a rat incisional wound model revealed that LAS-G accelerated wound closure, enhanced collagen deposition, and improved tissue regeneration. The synergistic effect of LA and SA contributes to improved gelation and biological properties, positioning LAS-G as a promising approach for advanced wound care. These findings indicated that LAS-G provides a safe, effective, and multifunctional strategy for promoting wound healing and tissue repair.

Received 6th February 2026,
Accepted 26th April 2026

DOI: 10.1039/d6ma00175k

rsc.li/materials-advances

1. Introduction

Regeneration/repair is the innate ability of all organisms that occurs after any injury or accident. Nevertheless, wound/tissue healing is an intricate process involving a tight coordination between proliferation, cell migration, matrix deposition and remodelling, along with inflammation and angiogenesis.[1] This process can take several days to months depending upon the severity of the damage. Meanwhile, open wounds can invite several infections, inflammation, and compromised skin barrier function.[2] Therefore, the synthesis of an effective and strategic material is required that has the dual functionality of both providing protection and improved healing.

In recent years, bioadhesive glues or hydrogels have gained tremendous attention for wound healing. These biological glues have the ability to adhere severe wounds while providing a healing microenvironment and protection from bacterial infection.[3,4] In this regard, natural macromolecules as well as small molecules have been widely explored for wound healing applications because of their inherent biocompatibility and biodegradability.[2,5–8] However, the hydrogels made of native macromolecules usually lack functional attributes (antioxidant, anti-inflammatory and antibacterial effects), which hinders their direct application. In light of this, α-lipoic acid (LA) has been extensively utilized as a therapeutic agent and dietary supplement for oxidative stress-related diseases. Structurally, LA contains a strained five-membered disulfide ring that can undergo ring-opening polymerization (ROP) under appropriate conditions, enabling the formation of polymeric or supramolecular networks with unique mechanical and self-healing properties.[9,10] The ROP of LA can be achieved by several methods, including thermal and photo-initiated radical polymerization, thiolate-initiated anionic polymerization, or acid-catalysed cationic polymerization.[11] Among all, the most convenient and solvent free bulk approach is thermal triggered ROP; however, the resultant polymerization is metastable due to reverse closed loop-depolymerization at room temperature.[11,12] Moreover, native poly-LA hydrogel has poor adhesion and rheological attributes. Therefore, to improve stability and adhesion attributes, it is essential to add components which enhance the

[a] *Dietetics and Nutrition Technology Division, CSIR-Institute of Himalayan Bioresource Technology, Palampur, 176061, Himachal Pradesh, India. E-mail: ankitsaneja@ihbt.res.in, ankitsaneja.ihbt@gmail.com; Tel: +91-1894-233339x485*

[b] *Academy of Scientific and Innovative Research (AcSIR), Ghaziabad, 201002, India*

crosslinking, such as various double-bond monomers, metal ions, ionic liquids, chlorinated organic solvents, and dopamine.[8] Nevertheless, stabilizing poly-LA hydrogels with toxic organic crosslinking agents or heavy metal ions may restrict their *in vivo* applications.[13,14] Thus, developing a novel preparation method for LA-based hydrogels is desirable to harness LA's therapeutic benefits.

Poly-LA-based hydrogels have been developed using polyphenols such as tannic acid and gallic acid as crosslinkers to stabilize LA polymerization.[2,10] In this study, we hypothesized that the incorporation of syringic acid (SA, natural phenolic compound) as an intrinsic multifunctional additive would enhance the crosslinking, adhesion and functional properties of poly-LA hydrogels through intermolecular interactions. SA is known to exhibit prominent antioxidant, anti-inflammatory, and antibacterial activities and has been reported to accelerate wound healing processes by promoting reepithelization.[15–17] Importantly, the phenolic hydroxyl and carboxyl groups of SA can participate in hydrogen bonding and ionic interactions, facilitating the formation of a multifunctional hydrogel. The interaction between SA and LA shows potential for creating novel adhesive hydrogels, integrating the advantages of both polyphenols and poly-sulphur.[2]

In this work, we report a facile, green strategy to synthesize poly-LA–SA hydrogel (LAS-G) for wound-healing applications. The synergistic presence of carboxylate and phenolic groups enhances hydrophilicity, intermolecular interactions, and adhesivity. The effects of SA concentration on gelation behaviour and adhesion were systematically investigated. The resultant hydrogel was characterized for rheology and molecular interaction *via* nuclear magnetic resonance spectroscopy (NMR), X-ray diffraction (XRD), and X-ray photoelectron spectroscopy (XPS). The functional attributes of the hydrogels were investigated by DPPH as well as an ABTS free radical scavenging assay, and their antibacterial activity against *Staphylococcus aureus* (*S. aureus*) and *Escherichia coli* (*E. coli*) was observed. Furthermore, the wound healing efficacy of the hydrogels was assessed using a linear incision wound model in rats.

2. Materials and methods

2.1. Materials

(±) α-Lipoic acid (LA, Mw: 206.33 g mol^{-1}, CAS no.: 1077-28-7) and Tris-base (Mw: 121.14 g mol^{-1}, CAS no. 77-86-1), and 1,1-diphenyl-2-picrylhydrazyl (DPPH, Mw: 394.32 g mol^{-1}, CAS no. 1896-66-4) were procured from Sigma-Aldrich (Missouri, USA). Syringic acid (SA, Mw: 198.17 g mol^{-1}, CAS no.: 530-57-4) was purchased from BLD Pharmatech Pvt Ltd (Telangana, India). 2,2′-Azino-bis(3-ethylbenzothiazoline-6-sulphonic acid) (ABTS, Mw: 514.6 g mol^{-1}, Cas No: 30931-67-0) was procured from MP Biomedicals. Povidone iodine ointment (USP, 5% w/w) was purchased from a local market. The microbial strains *Staphylococcus aureus* (*S. aureus*, MTCC 96) and *Escherichia coli* (*E. coli*, MTCC 43) were procured from CSIR-Institute of Microbial Technology, India. All reagents used were of analytical grade, unless stated otherwise.

2.2. Optimization and preparation of the poly-LA–SA hydrogel

The poly-LA hydrogel (LA-G) was prepared by dissolving 500 mg of tris base in 2 mL of MQ water, then adding 1 g of LA and mixing thoroughly. The resulting viscous solution was heated at 70 °C for 2 hours. Afterward, the solution was subjected to freeze–thaw cycles, with freezing at −20 °C for 1 hour and thawing at 25 °C to obtain the LA-G.[2]

The poly-LA–SA hydrogel (LAS-G) was prepared at varying weight ratios of LA : SA, *viz.*, 1 : 0.05, 1 : 0.1, and 1 : 0.2, to determine the composition with optimal adhesion properties. Initially, 500 mg of tris base was dissolved in 2 mL of MQ water. The aforementioned amount of SA was added (*i.e.*, 50, 100, and 200 mg), followed by the addition of 1 g of LA. The mixture was vortexed and heated at 70 °C for 2 hours. The obtained solution was frozen at −20 °C for 1 hour and later thawed at 25 °C to yield LAS-G. The gels were then qualitatively assessed for adhesivity using different materials such as plastic, glass, steel, wood, and leaf.[18]

2.3. Rheological evaluation of the hydrogel

The rheological behaviour of both the LA-G and LAS-G hydrogels was examined using a rheometer (Anton Paar, Austria) fitted with a parallel plate geometry (50 mm diameter, 1 mm gap). Approximately 2 g of each hydrogel sample was carefully placed on the lower plate to fully cover the 50 mm diameter, and the upper plate was lowered to the desired gap to ensure uniform contact without air entrapment. The samples were allowed to equilibrate for 5 minutes prior to measurement. The frequency sweep tests were carried out to record the storage modulus (G') and loss modulus (G''), to evaluate the viscous deformation and gelation behaviours of the hydrogels.[18]

2.4. Characterization of the developed LA-G and LAS-G

The developed hydrogel was analyzed for possible molecular interaction using NMR spectroscopy. The ^{1}H NMR spectra of LA, SA, LA-G, and LAS-G were recorded in DMSO-d_6 using a 400 MHz NMR spectrophotometer (JEOL, NM-70010S4L1). The ^{1}H spectra were assessed for ROP and cross-linking required for hydrogel formation.[19]

The X-RD patterns of LA-G and LAS-G, along with free LA and SA, were obtained using a diffractometer coupled with a Cu-Kα radiation source (Rigaku, MiniFlex). The diffractograms were obtained with an angular range of 2θ from 5 to 60°, with a step size of 0.02° and a scanning rate of 10° per min.[20]

The surface morphology and elemental composition of the gels were characterized using a scanning electron microscope (SEM) equipped with an energy dispersive X-ray (EDX) detector (Hitachi, S-3400N, Tokyo, Japan). Prior to analysis, the gel samples were lyophilized to remove residual moisture. The samples were placed on a metal stub with the help of double-sided adhesive carbon tape, and subsequently coated with gold using ion sputtering (Hitachi, E-1010, Tokyo, Japan). The micro-images of the gels were obtained at an accelerating voltage of 15 KV under vacuum, and subsequently, EDX spectra were recorded.[21]

To further analyse the elemental composition of the LA-G and LAS-G, XPS spectra were obtained using an X-ray photoelectron spectrometer (Thermo Scientific, NEXSA Surface Analysis). In brief, approximately 20 mg of the sample was taken and irradiated with an X-ray beam generated from a Cu-kα source. Simultaneously, the kinetic energy of electrons emitted from the upper 1–10 nm layer of the sample surface was detected with a NaI scintillation detector.[18]

2.5. Determination of the antioxidant potential of the developed LA-G and LAS-G

The antioxidant activity of LA-G and LAS-G was evaluated using both DPPH and ABTS radical scavenging assays.[22] For evaluation of DPPH radical scavenging activity, a fresh DPPH solution (100 μM) was prepared in methanol. Briefly, 20 mg of LA-G and LAS-G was accurately weighed and dissolved in 1 mL of methanol, followed by dilution to get a specified concentration of the hydrogel (1000–62.5 μg mL^{-1}). The hydrogel samples at specific concentrations were mixed with DPPH solution in a 1 : 2 (sample:DPPH, v/v) ratio and incubated in the dark at 37 °C for 30 minutes. After incubation, the absorbance of the samples was recorded at 517 nm and % DPPH radical scavenging was determined using eqn (1).

$$\%\,\text{DPPH radical scavenging activity of hydrogel} = \frac{A_c - A_t}{A_c} \times 100 \quad (1)$$

where A_c is the absorbance of the control sample and A_t is the absorbance of the test sample (hydrogel).

Furthermore, the ABTS radical scavenging activity of the hydrogels was also evaluated. To prepare the stock solution of ABTS free radicals, ABTS salt solution (7 mM) was mixed with potassium persulfate (2.45 mM) and incubated in the dark for 16 hours. Subsequently, 100 μL of hydrogel sample (concentration ranging from 2000–125 μg mL^{-1}) was mixed with 1.9 mL of working ABTS solution, protected from light and incubated for 6 minutes at RT.[22] The absorbance of the solution was recorded at 734 nm and % ABTS radical scavenging activity was determined using eqn (2).

$$\%\,\text{ABTS radical scavenging activity of hydrogel} = \frac{A_c - A_t}{A_c} \times 100 \quad (2)$$

where A_c is the absorbance of the control sample and A_t is the absorbance of the test sample (hydrogel).

2.6. Antibacterial activity analysis of the developed hydrogels

The antibacterial efficacy of LA-G and LAS-G was evaluated against Gram-positive-*S. aureus* (MTCC 96) and Gram-negative *E. coli* (MTCC 43) bacterial strains. Initially, the *S. aureus* and *E. coli* strains were cultured in nutrient broth and Luria broth, respectively, at 37 °C with continuous agitation and the optical density of the bacterial cultures were adjusted to 10^8 CFU mL^{-1}.[23] Subsequently, the hydrogel samples (30 mg mL^{-1}) were immersed in 25 mL of broth, either Luria (*E. coli*) or nutrient broth (*S. aureus*), and incubated at 37 °C with continuous shaking for 12 hours. After incubation, 100 μL of the bacterial suspension was serially diluted to 10^{-6} using phosphate-buffered saline (PBS), and uniformly spread onto solid agar plates (nutrient and Luria Agar). Untreated bacterial suspensions were considered as control groups. The plates were incubated at 37 °C for another 12 hours and the number of colonies was counted with a Handheld digital colony counter (HIMEDIA) and CFU mL^{-1} was calculated using the following equation:

$$\text{CFU/mL} = \frac{(\text{No. of colonies} \times \text{dilution factor})}{\text{Volume of culture plated}} \quad (3)$$

2.7. Animal care and experimental design

The wound healing efficacy of LA-G and LAS-G was evaluated using the linear incision wound model in rats. The male rats (wistar rats weighing 150–200 gm) were randomly divided into four groups (n = 6) and housed under standard laboratory conditions (temperature 22 ± 3 °C, relative humidity 40–60%, and 12 h light/dark cycle) at the institutional animal facility. The animals were provided with *ad libitum* feed and water. The experimental protocol was duly approved by the Institutional Animal Ethical committee (IAEC) with approval no. IHBT-IAEC-0823-P06.

2.7.1. Incisional wound rat model. The rats were anesthetized by intraperitoneal administration of ketamine 70 mg Kg^{-1} (Ketapil, Psychotropics India Ltd) and xylazine 10 mg Kg^{-1} (Sigma-Aldrich, USA).[24] The fur on the dorsal skin surface was removed and the skin surface was cleaned with 70% ethanol. An incision of 20 mm was made with a scalpel followed by application of ~0.2 mL hydrogel.[4] The wound was monitored daily with application of the hydrogel for a period of 10 days. The standard group received ~0.2 mL of povidone–iodine ointment on the wound.[25] On the 10^{th} day, percent wound closure was determined using the following equation:

$$\text{Wound closure}\,(\%) = \frac{\text{Initial incision length} - \text{final incision length}}{\text{Initial incision length}} \times 100 \quad (4)$$

Furthermore, the animals were sacrificed and the wound tissue along with the surrounding skin was collected for histological analysis.

2.7.2. Histopathology of the wounded skin. The collected skin tissues were fixed in 10% v/v neutral buffered formalin, and subsequently processed for embedding in paraffin blocks. Afterwards, sectioning of the skin tissue was performed with the help of a microtome (Thermo Fisher Scientific, MA, USA) set at a thickness of 5 μm and sections were collected on glass slides. The haematoxylin and eosin staining of the tissue sections were performed and images were captured using bright-field microscopy (BX35, Olympus, Tokyo, Japan) to analyse the structural integrity of the skin.[26] Furthermore, for the evaluation of collagen deposition and tissue remodelling, the tissue sections were stained with Masson's trichome and picrosirius red staining. The relative collagen deposition with

respect to the control group was determined by quantifying % area of aniline blue in masons trichome stained sections and the % area of red staining in the picrosirius red stained section, using ImageJ software.[26,27]

2.8. Statistical analysis

The statistical analysis was performed with GraphPad Prism 10.6.1 (GraphPad software Inc., CA, USA) using analysis of variance (one-way/two-way ANOVA) followed by Tukey's post-hoc test to assess the significance difference (p value < 0.05). The results are represented as mean ± standard deviation (SD).

3. Results and discussion

3.1. Development and rheological evaluation of LA-G and LAS-G

LA undergoes ROP of its dithiolane moiety upon heating, leading to the formation of a long chain of poly-LA (LA-G) through disulfide bonding. LA readily solubilizes at higher concentration in aqueous solution in the presence of tris base, which accelerates the thermal ROP process.[2,8] However, the resultant poly-LA exhibits metastable properties due to closed loop depolymerization, which restricts its therapeutic applications.[18,28] This depolymerization usually occurs due to lack of intermolecular interaction and weak binding affinity between LA monomers.[28] Herein, we hypothesized that the metastable state of the LA polymer may be stabilized with incorporation of SA. SA is a phenolic compound having different functional groups that may form intermolecular non-covalent interactions with LA monomers and thereby act as a cross-linking agent (Fig. 1).[15] Therefore, three LAS-G hydrogels were developed with copolymerization of LA and different concentrations of SA. The LA-G exhibited a viscous solution-like consistency, whereas the consistency of LAS-G differs with varying SA ratio (Table 1).

The qualitative adhesivity assessment of the developed hydrogels was performed using different materials, *i.e.* plastic,

Table 1 Composition of hydrogels developed with varying concentrations of SA

Gel (LA : SA, w/w)	LA (mg)	SA (mg)	Molar ratio (LA : SA)	Tris-base (mg)	MQ water (mL)
LA-G (1 : 0)	1000	—	—	500	2
LAS-G (1 : 0.05)	1000	50	19.20	500	2
LAS-G (1 : 0.1)	1000	100	9.68	500	2
LAS-G (1 : 0.2)	1000	200	4.80	500	2

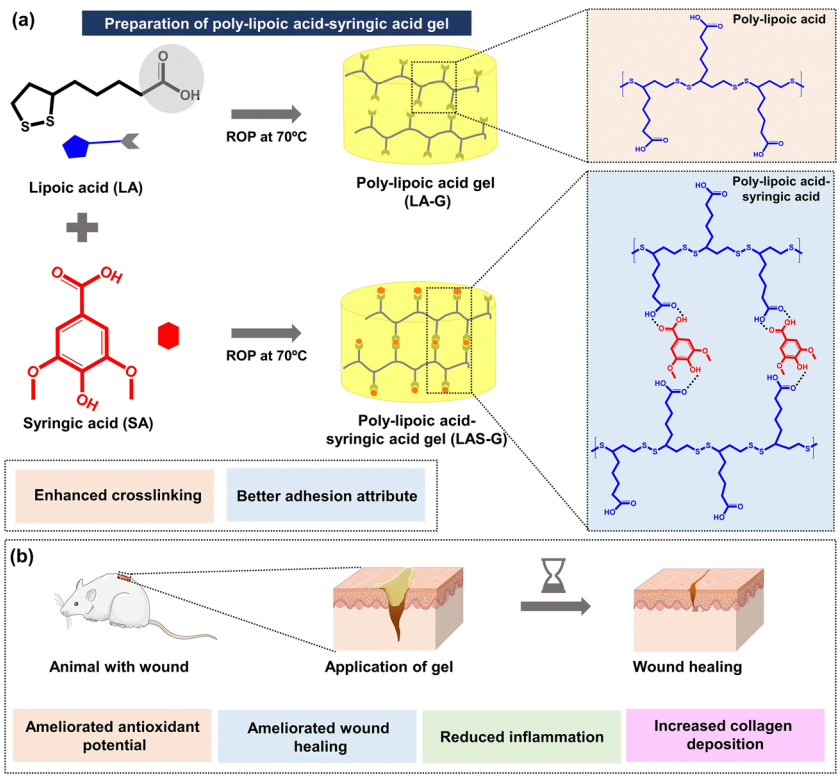

Fig. 1 Preparation and biomedical application of poly-lipoic acid-syringic acid gel. (a) Schematic illustration of the synthesis of poly-lipoic acid gel (LA-G) and poly-lipoic acid–syringic acid gel (LAS-G). Lipoic acid (LA) undergoes ring-opening polymerization (ROP) at 70 °C to form a crosslinked poly-lipoic acid network. Incorporation of syringic acid (SA) during ROP produces LAS-G with increased gelation and superior adhesive properties, as depicted by the polymer network structures. (b) Schematic representation of the *in vivo* wound-healing application. The gel is applied to a skin wound to promote wound closure. The observed therapeutic effects include elevated antioxidant activity, accelerated wound healing, reduced inflammation, and enhanced collagen deposition.

glass, steel, wood, and leaf (Fig. 2a).[4,29] The adhesivity assessment revealed that LAS-G having 1 : 0.1 w/w LA : SA ratio holds superior adhesivity among all hydrogels by adhering all aforementioned materials. Therefore, LAS-G (1 : 0.1 w/w) was selected for further characterization and wound healing assessment. While these substrates provide insight into interfacial adaptability and comparative adhesion trends, they do not predict wound closure.

The rheological evaluation of LA-G and LAS-G was assessed using frequency-sweep test. The LA-G demonstrated a lower storage modulus (G') than loss modulus (G''), indicating predominantly viscous deformation behaviour (Fig. 2b.i).[18] In contrast, LAS-G initially exhibited lower G' than G''; however, a G' to G'' crossover was observed at lower frequency than in LA-G, indicating enhanced gelation and reinforcing of the hydrogel network (Fig. 2b.ii).[30] This behaviour may possibly be attributed to enhanced cross-linking facilitated by non-covalent interaction with SA.[20,31] Additionally, the rheological behaviour of LAS-G was also analysed at 90 °C, which demonstrated higher G' value than G'', indicating gelation and the formation of a dense cross-linked hydrogel network at a higher temperature (Fig. 2b.iii). This observation supports thermally initiated ROP as a suitable process for the formation of a hydrogel network between SA and LA. The improved adhesivity and gelation of LAS-G in comparison to LA-G can be attributed to possible cross-linking of the poly-(LA) chain through intermolecular interactions with SA.[13,18,20]

3.2. Characterization of LA-G and LAS-G hydrogels

3.2.1. Nuclear magnetic resonance spectroscopy. The ^{1}H NMR spectra of the hydrogels were analysed to confirm ROP and intermolecular interaction of poly-LA with SA. The ^{1}H spectrum of LA demonstrated characteristic peaks in the range of 3.59 to 2.40 ppm and 1.87 ppm corresponding to the protons of the dithiolane moiety. Additionally, peaks at 2.19, 1.87, 1.52 and 1.37 ppm were attributed to protons present in the LA carbon chain.[19,32] The ^{1}H spectrum of SA exhibited a characteristic peak at 12.57 and 9.18 ppm corresponding to the –COOH group and –OH group, respectively. The protons of the aromatic ring demonstrated a characteristic peak at 7.19 ppm, while the peak for –OCH_3 group protons appeared at 3.79 ppm.[33] The ^{1}H spectrum of LA-G demonstrated peaks at 3.84 and

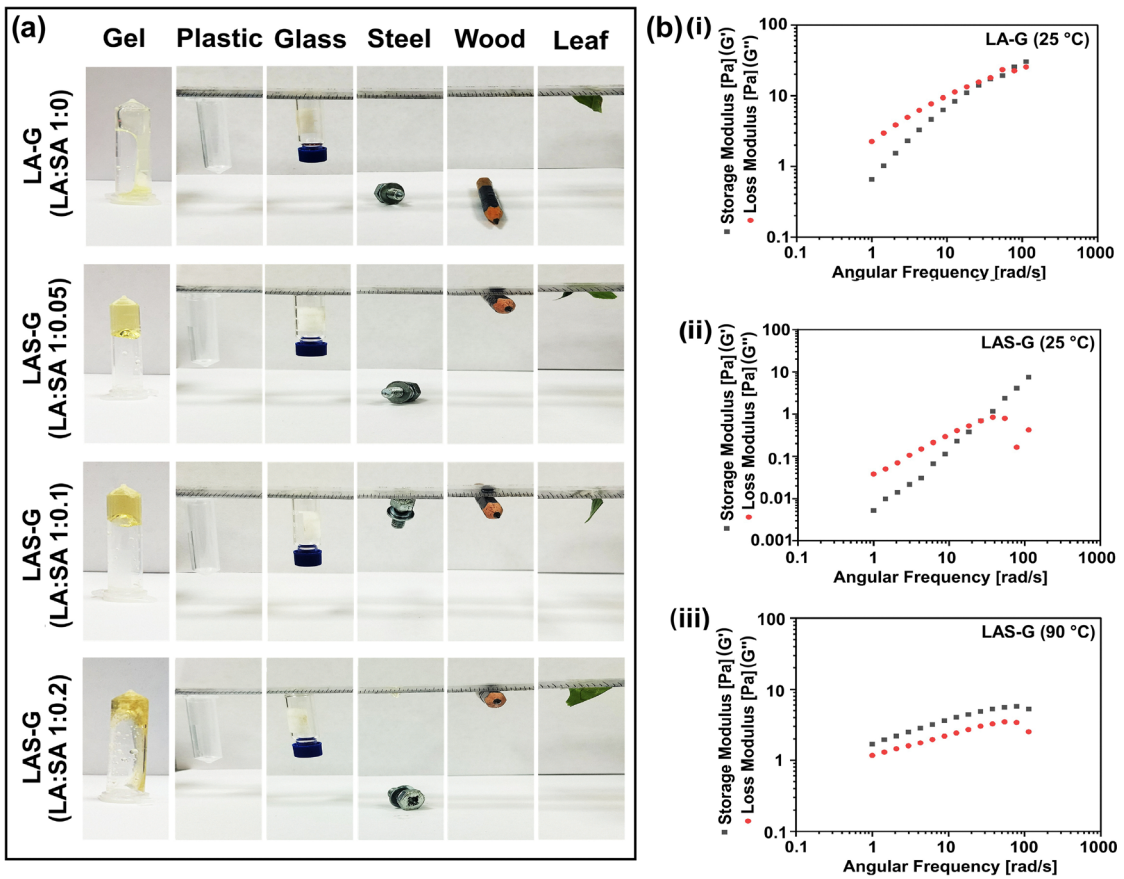

Fig. 2 Adhesion and rheological properties of LA-based gels on various substrates. (a) Images displaying the adhesion performance of LA-G and LAS-G formulations with different LA : SA ratios (1 : 0, 1 : 0.05, 1 : 0.1, and 1 : 0.2) on substrates such as gel, plastic, glass, steel, wood, and leaf surfaces. The gels' capacity to adhere to and suspend objects with diverse materials and surface characteristics is demonstrated. (b) Dynamic rheological analysis: frequency-dependent storage modulus (G', black squares) and loss modulus (G'', red circles) are plotted as functions of angular frequency. (i) LA-G at 25 °C, (ii) LAS-G at 25 °C, and (iii) LAS-G at 90 °C. The results highlight the viscoelastic properties of the gels and the influence of SA incorporation and temperature on viscoelastic behaviour.

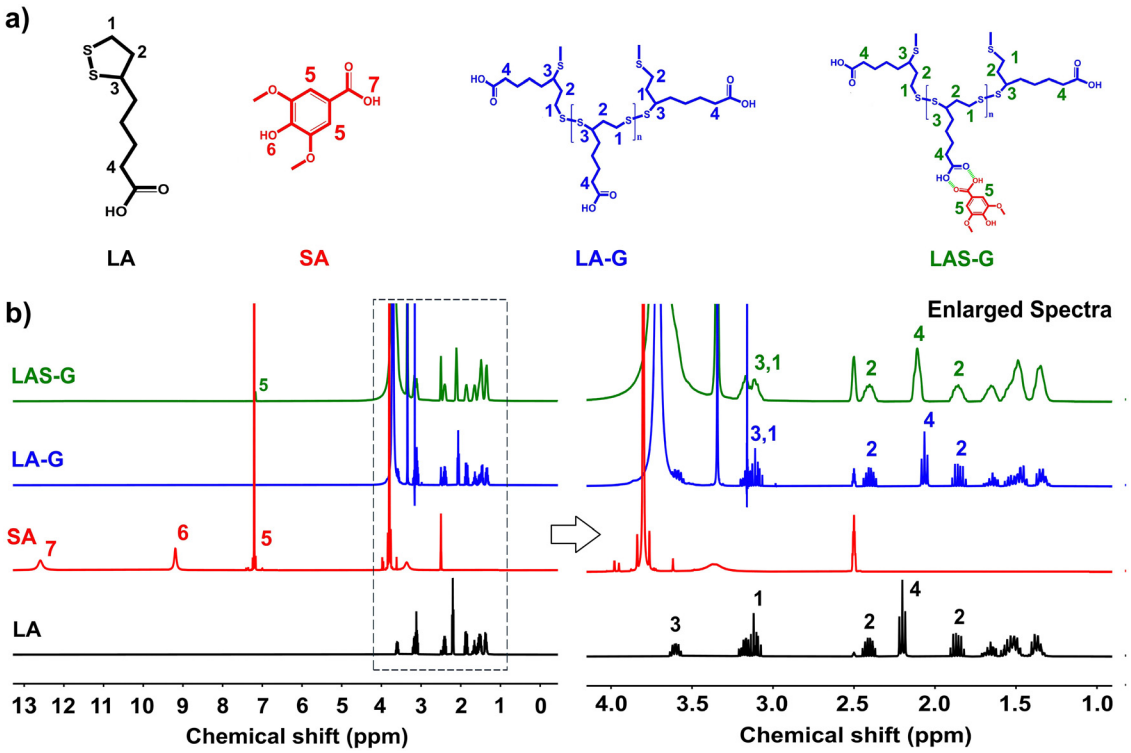

Fig. 3 (a) Chemical structures of lipoic acid (LA), syringic acid (SA), LA-gel (LA-G), and lipoic acid-syringic acid gel (LAS-G), with proton numbering for NMR peak assignment indicated. (b) ^{1}H NMR spectra of LA, SA, LA-G, and LAS-G obtained in DMSO-d_6. Characteristic resonances for the numbered protons are labelled. The boxed region highlights aliphatic and gel-related signals, indicating successful SA incorporation. Enlarged spectra on the right display peak shifts and signal broadening, suggesting gel formation.

3.36 ppm attributed to the amine group of the tris base and water, respectively. Although the ^{1}H spectrum of LA-G was similar to that of LA, a pronounced upfield shift in the peak from 2.19 to 2.04 was observed, along with a minor shift in the peaks ranging from 1.63 to 1.45 ppm. These variations in chemical shift indicated a reduction in bond strain following opening of the dithiolane ring of LA.

The ^{1}H spectrum of LAS-G demonstrated peaks at 3.78 and 3.44 ppm corresponding to the tris base and water, respectively. Furthermore, a distinct peak at 7.27 ppm corresponding to the OH-group from SA was observed. The peaks corresponding to the protons of the dithiolane ring of LA were merged in the LAS-G spectrum, signifying the ROP of the LA.[19,34] Moreover, the peak corresponding to the OH-group of the carboxylic acid of the SA disappeared in the proton spectra of LAS-G, suggesting its possible interaction, such as hydrogen bonding with the LA molecule, which aided in the persistence of the ROP (Fig. 3).[28] This non-covalent interaction of the SA with LA in the LAS-G may possibly be responsible for its improved adhesivity and stability in comparison to LA-G.

3.2.2. X-ray diffraction pattern analysis. The XRD pattern of LA exhibited prominent reflections at 2θ values of 8.3°, 23.7°, 24.4°, 26.04°, and 32.59°.[35] Likewise, SA showed distinct diffraction peaks at 2θ values of 11.5°, 12.6°, 13.5°, 22.9°, and 34.3°, indicating the crystalline nature of both compounds.[36] These characteristic peaks of LA and SA disappeared in both LA-G and LAS-G, indicating amorphous nature of the hydrogels. This change in the state from crystalline to amorphous upon gel formation may possibly be due to the self-polymerization of LA and intermolecular interaction with SA (Fig. 4a). Similar findings have been reported for poly-LA hydrogels, where polymerization of LA leads to a transition from a crystalline to an amorphous structure.[37]

3.2.3. Surface morphology and elemental composition of LA-G and LAS-G. The surface morphology of LA-G and LAS-G was analysed by SEM. The microphotograph of LA-G demonstrated a smooth and continuous surface without cracks as a result of the formation of viscous phase resulting from polymerization. Conversely, LAS-G demonstrated a dense interconnected microstructure as an attribute to the ROP and intermolecular interaction with SA (Fig. 4b).[13] This interconnected porous surface of LAS-G contributed to its improved gelation, making it suitable for applications such as wound healing.[13] The EDX spectra for both LA-G and LAS-G revealed sulphur as the major element followed by carbon and oxygen (Fig. S5, SI).[2]

Furthermore, the structural characteristics and chemical composition of LA-G and LAS-G were also confirmed with XPS analysis.[2,18] The XPS survey scan of the hydrogels demonstrated major characteristic peaks at binding energies of ~164 and

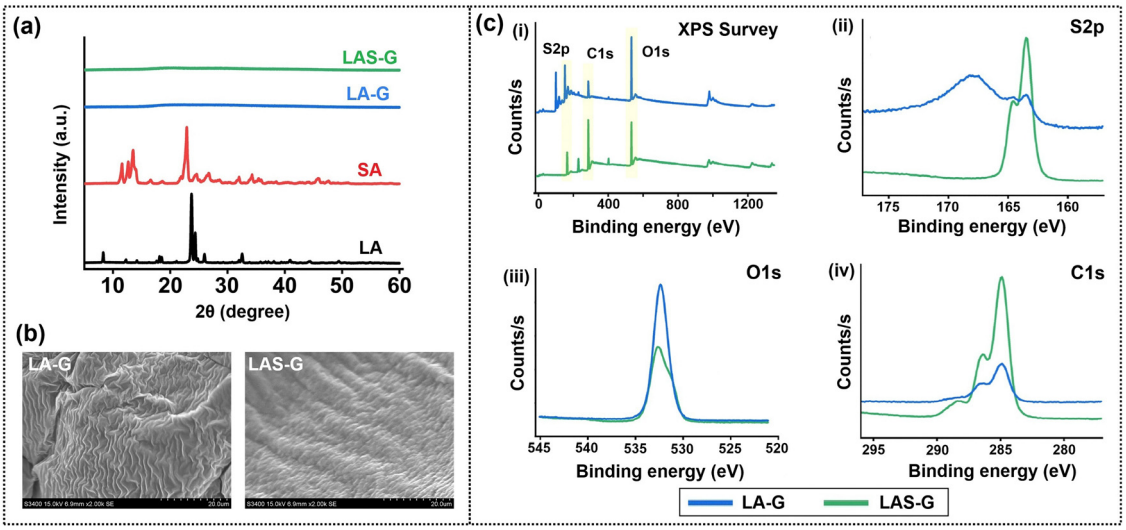

Fig. 4 Structural, morphological, and chemical characterization of LA-based materials. (a) X-ray diffraction (XRD) patterns of LA, SA, LA-G, and LAS-G reveal the crystalline nature of the native components and the predominantly amorphous structure following composite formation. (b) Scanning electron microscopy (SEM) images of LA-G and LAS-G show differences in surface morphology and texture after modification (scale bar: 20 μm). (c) X-ray photoelectron spectroscopy (XPS) analysis of LA-G and LAS-G includes: (i) survey spectra confirming elemental composition, (ii) high-resolution S 2p spectra, (iii) high-resolution O 1s spectra, and (iv) high-resolution C 1s spectra, which indicate changes in surface functional groups and chemical states resulting from SA incorporation.

~168 eV corresponding to S 2p, along with peaks at ~532 and ~285 eV attributable to O 1s and C 1s, respectively (Fig. 4c.i). Additionally, the characteristic peak for N 1s can been seen, attributed to the presence of tris base (Table S1, SI). Moreover, the high resolution scans of S 2p, O 1s and C 1s were recorded to elucidate the interaction mechanism.[18] The S 2p spectra of the hydrogels were analysed with non-linear curve fitting to obtain a deconvoluted spectra (Fig. S6, SI). The S 2p spectrum of LA-G demonstrated a characteristic peak for disulfide at 164.3 eV and a peak at 163.4 eV corresponding to aliphatic–sulphur affirming ROP. Additionally, a broad peak at 168.1 eV was observed attributed to the oxidized sulphur atom. In contrast, the S 2p spectrum of LAS-G demonstrated two major peaks, one at 164.5 eV assigned to the disulfide bond and a relatively intense peak at 163.4 eV corresponding aliphatic sulphur (Fig. 4c.ii). Furthermore, the atomic percentage of the S 2p of LAS-G was relatively lower than that of LA-G, likely due to the presence of SA, which mitigated the oxidation of the sulphur atom (Table S1, SI). Overall these observations indicate efficient ROP of LAS-G compared to LA-G, leading to stronger intermolecular interaction.[2]

The O 1s spectrum of LA-G demonstrated a single characteristic peak for C═O at 532.3 eV. Conversely, the O 1s spectrum of LAS-G demonstrated two peaks, one at 532.6 eV corresponding to the C═O and another at 531.1 eV corresponding to the C–O group, indicating the possibility of non-covalent interaction, contributing to stabilizing the hydrogel network (Fig. 4c.iii).[18] In the high resolution C 1s spectrum of LA-G, the characteristic peaks at 288, 286.6, and 284.8 eV correspond to the C═O, C–O, and C–C, respectively. The C 1s spectrum of LAS-G demonstrated a characteristic peak of C═O at 288.4 eV and a relatively intense peak at 286.3 eV for C–O, indicating non-covalent interactions, such as hydrogen bonding, along with a peak at 284.8 eV corresponding to C–C (Fig. 4c.iv).[13]

Collectively, the surface morphology and XPS analysis demonstrated that LAS-G possesses an interconnected, irregular, porous surface, possibly attributed to the non-covalent interaction between LA and SA.

3.3. Antioxidant and antibacterial effect of LA-G and LAS-G

Generally, reactive oxygen species (ROS) are produced as part of the host defence response and, at low concentrations, play an essential role in protective mechanisms. Paradoxically, excessive ROS generation exacerbates the cellular damage in chronic wounds.[38,39] Therefore, the hydrogel implicated for wound healing applications should hold strong ROS scavenging antioxidant activity.

The DPPH and ABTS assays are commonly employed and affordable methods for determining the antioxidant potential of bioactive molecules.[22,40] The results of the DPPH radical scavenging assay demonstrated that LAS-G exhibited significantly higher ($p < 0.05$) radical scavenging than LA-G at all tested concentrations (ranging from 62.5–1000 μg mL^{-1}), with 92.33 ± 0.41% scavenging at the highest concentration compared to LA-G (7.29 ± 0.47%) (Fig. 5a). Similarly, at all tested concentrations (ranging from 125–2000 μg mL^{-1}), LAS-G demonstrated significantly higher % ABTS radical scavenging activity than LA-G ($p < 0.05$), with 70.92 ± 0.32% scavenging at the highest concentration compared to LA-G (4.16 ± 0.70%) (Fig. 5b). This significant increase in antioxidant activity of LAS-G compared to LA-G, was likely associated with the abundance of phenol groups attributable to the presence of SA.[15,41]

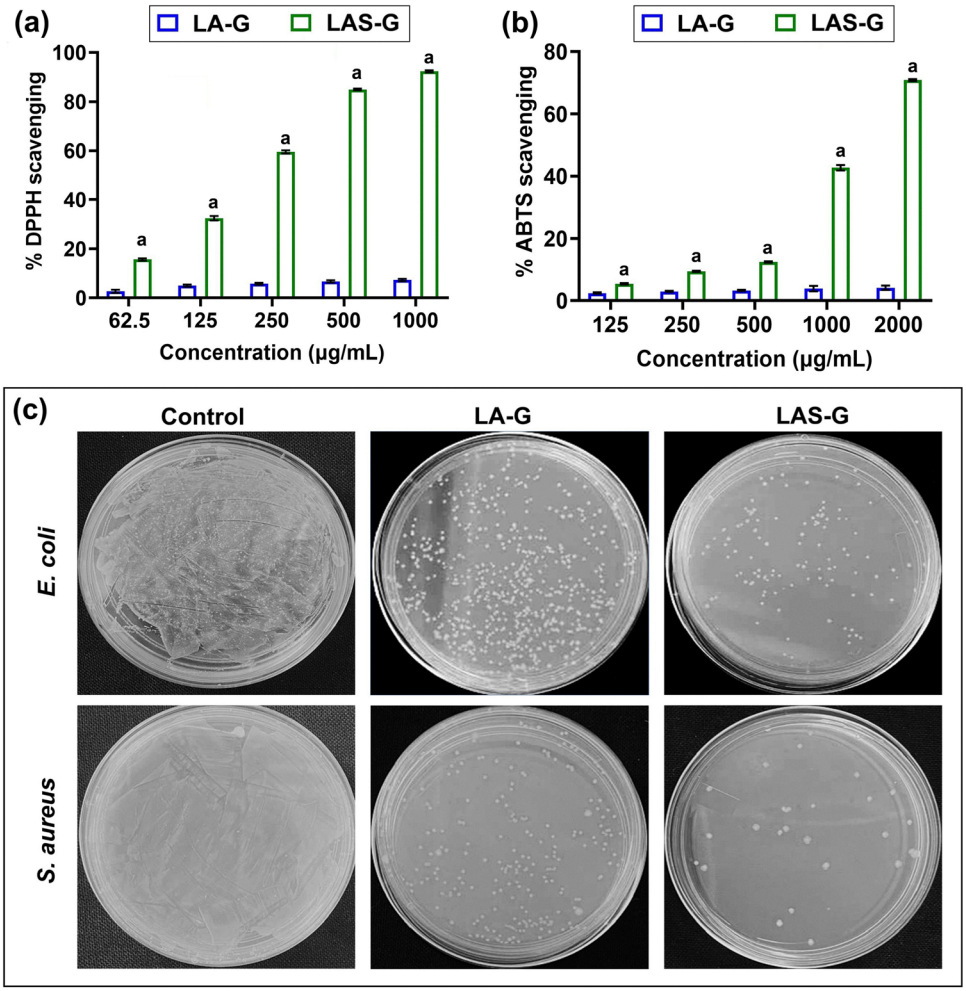

Fig. 5 Antioxidant and antibacterial activity of LA-based gels. (a) %DPPH scavenging activity of LA-G and LAS-G formulations. (b) %ABTS scavenging applications of LA-G and LAS-G formulations. (c) Photographs of survival colonies of *E. coli* and *S. aureus* bacterial strains on agar plate after 12 h treatment at 30 mg/mL concentrations of LA-G and LAS-G formulations. a represents significant difference from LA-G ($p < 0.05$)

The hydrogel implicated for wound healing should protect the wound from bacterial infection as well. The bacterial infection can generate excessive ROS, which can obstruct the healing process.[42] Therefore, the *in vitro* antibacterial activity of both LA-G and LAS-G was tested against *S. aureus* (Gram-positive) and *E. coli* (Gram-negative) (Fig. 5c). The control plate demonstrated confluent bacterial growth (lawn), confirming no inhibitory effect. The LA-G treated plate exhibited 2.3×10^6 CFU mL^{-1} against *S. aureus* and 3.0×10^6 CFU mL^{-1} against *E. coli*, indicating a weak inhibitory effect. The LAS-G showed a strong inhibitory effect with 3.0×10^5 CFU mL^{-1} against *S. aureus* and 1.25×10^6 CFU mL^{-1} against *E. coli*. The improved antibacterial activity of LAS-G was likely associated with SA, as its phenolic exoskeleton exhibits strong antibacterial activity against various pathogens, both Gram-positive and Gram-negative bacteria.[15,33] Similar enhancements in antibacterial efficacy have been reported for LA-based hydrogels cross-linked with tannic acid and gallic acid.[10,21,43]

Overall, the presence of SA enhanced the antioxidant and antibacterial activity of LAS-G, desired for modulating the microenvironment of the wound.

3.4. Incisional wound healing and skin structure integrity

The *in vivo* wound healing of LA-G and LAS-G was evaluated with a linear incision model in Wistar rats.[2,4] The wound healing capacity of the hydrogels was assessed after 10 days of treatment and % wound closure was evaluated (Fig. 6a). The % wound closure for the control group was 28.54 ± 4.65% whereas the standard group treated with povidone–iodine had demonstrated significantly high (47.71 ± 6.12%) wound closure. The group treated with LA-G showed a less pronounced effect than the standard group with 35.31 ± 7.16% wound closure. However, the group treated with LAS-G demonstrated 69.20 ± 10.42% wound closure significantly higher ($p < 0.05$) than both the standard as well as the LA-G group (Fig. 6b and c and Fig. S7, SI). The improved wound healing with LAS-G was possibly attributed to the presence of SA and its non-covalent interaction with the LA, which collectively improved its viscoelastic and adhesive attributes while simultaneously ameliorating its antioxidant and antibacterial activity, thereby promoting accelerated wound healing.[2,18]

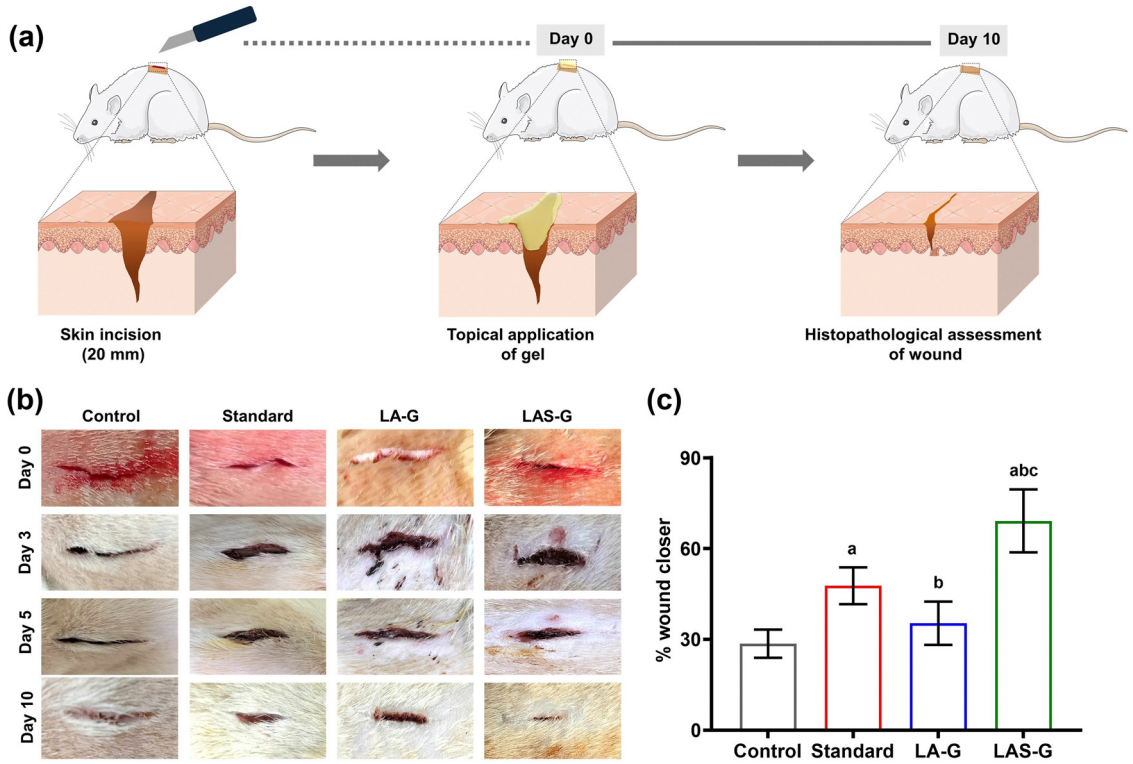

Fig. 6 *In vivo* wound-healing evaluation of gel formulations in a rat incisional wound model. (a) Schematic illustration of the experimental design. A full-thickness linear skin incision (20 mm) was created on the dorsal region of rat (Day 0), followed by topical application of the respective gel formulations. Wound-healing progression was monitored, and histopathological assessment was conducted on Day 10. (b) Representative macroscopic images of wounds from the control, standard, LA-G, and LAS-G groups were captured on Days 0, 3, 5, and 10 post-wounding. (c) Quantitative analysis of percentage wound closure on Day 10 for all groups. Data are shown as mean ± SD (n = 6). Different superscript letters (a–c) indicate statistically significant differences between groups ($p < 0.05$). a, b, c indicates compared to control, standard and LA-G respectively.

Furthermore, to investigate the wound healing efficacy of the hydrogels, skin tissue collected on day 10 post incisional wound was also processed for histological analysis (Fig. 7a). The haematoxylin and eosin staining of the skin tissues was performed to analyse the structural integrity of the wounded skin tissue following treatment. The control group demonstrated mild infiltration of inflammatory cells, and showed disrupted epidermis layer with granulation tissue formation. Conversely, the standard group treated with povidone–iodine demonstrated a milder infiltration of inflammatory cells than the control group, with repaired epidermal layer. The standard treatment showed increased granulation tissue as compared to the control. The LA-G group showed minimal presence of inflammatory cells and partial restoration of the epidermis layer; the effect was less pronounced than that of the standard group. However, wounds treated with LAS-G demonstrated restoration of the epidermis layer along with granulation tissue, with the presence of minimal inflammatory cells in the dermis. The presence of hair follicles further confirms the accelerated wound healing (Fig. 7b).[4,17,18] Similarly, treatment of linear incisional wounds in rats with LA-based hydrogels crosslinked with tannic acid has been shown to enhance wound healing.[2] In the present study, the accelerated wound closure observed with LAS-G is attributed to the synergistic effect of SA, which enhances gelation of the polymerized poly-LA hydrogel network compared to LA-G.

Furthermore, to evaluate the repair process and the collagen deposition in the wounded skin tissue following treatment, Masson trichome and picrosirius red staining were performed.[18,42] Treatment with LAS-G demonstrated a significant increase in collagen deposition, with a 2.12 ± 0.04-fold increase in aniline blue staining compared to the control. Moreover, this increase was also significantly higher than in the standard and LA-G group, with the appearance of hair follicles beneath the epithelium indicating accelerated wound healing. Meanwhile, less collagen fibrils with a random distribution were observed in the control group. Whereas the LA-G treated wound exhibited the least pronounced effect on collagen deposition compared to both the standard and LAS-G treatment with 1.40 ± 0.08-fold increase (Fig. 7c).[2,26] Collagen deposition was further validated with picrosirius red staining. The fold increase in the total collagen deposition was determined with respect to the control group. The standard group exhibited a 1.40 ± 0.01-fold increase in collagen deposition compared to the control group. The LA-G group demonstrated a similar trend as observed in the Masson trichrome staining, exhibiting a 1.21 ± 0.01-fold increase in collagen. However, The LAS-G-treated wound demonstrated a higher collagen deposition than the control, standard and LA-G group, with a 1.54 ± 0.03 fold increase in collagen, aligning with Masson trichome stained sections (Fig. 7d). The enhanced collagen deposition, with improved epidermal integrity, confirms

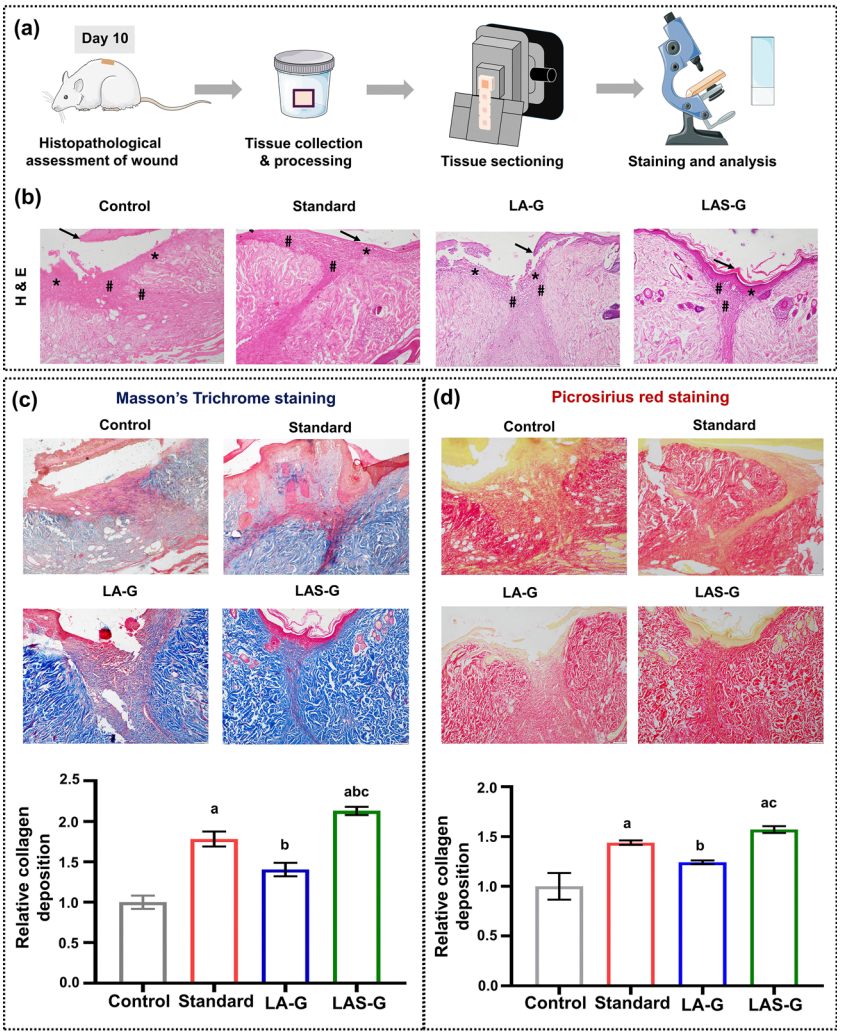

Fig. 7 Histopathological evaluation of wound healing on day 10. (a) Schematic illustration of the experimental workflow, including histopathological assessment, tissue collection and processing, sectioning, staining, and microscopic analysis (scale bar: 100 μm). (b) Representative haematoxylin and eosin (H&E) stained sections of wounded skin tissue from the control, standard, LA-G, and LAS-G groups demonstrate overall tissue architecture and re-epithelialization (indicates epithelium, # represents granulation tissue and * indicates inflammatory cells). (c) Masson's trichrome-stained sections from the four groups highlight collagen deposition (blue). The accompanying bar graph presents quantitative analysis of the relative collagen deposition. (d) Picrosirius red-stained sections under bright-field microscopy indicate collagen content and organization. The corresponding bar graph displays the quantified relative collagen deposition. Data are shown as mean ± SD (n = 3). Different letters above the bars indicate statistically significant differences between groups ($p < 0.05$). a, b, c indicates compared to control, standard and LA-G respectively.

the accelerated wound healing potential of LAS-G.[26] The improved wound healing observed with LAS-G compared to LA-G may possibly be attributable to the intermolecular interaction of poly-LA with SA, which enhanced the antioxidant and antibacterial effects as well as increased the collagen deposition.[2,17]

4. Conclusion

In summary, the poly-LA–SA hydrogel (LAS-G) demonstrated significant potential as an advanced wound care material. The combination of LA and SA formed a green hydrogel with improved viscoelasticity and adhesivity. LAS-G exhibited better antioxidant and antibacterial activity, effectively addressing key challenges in wound healing. *In vivo* rat model studies confirmed that LAS-G accelerates wound closure, promotes collagen deposition, and supports tissue repair more efficiently than control treatments. Comprehensive characterization validated its stable, cross-linked, and porous structure. Our study demonstrated that by harnessing the synergistic properties of LA and SA, LAS-G offers a safe, multifunctional approach to wound healing and tissue repair. These findings highlight the potential of LAS-G as a novel, effective, and environmentally friendly therapeutic platform for wound management. Although the present study demonstrates promising physicochemical and wound-healing properties, additional studies including quantitative adhesion analysis and advanced mechanistic investigations are required for translational validation.

Author contributions

Navneet Thakur: writing – original draft, investigation, methodology, and formal analysis. Ruchika: writing – original draft, investigation, methodology, and formal analysis. Neha Rana: writing – original draft, investigation, methodology, and formal analysis. Vikram Patial: writing – review and editing, methodology, and formal analysis. Ankit Saneja: writing – review and editing, supervision, project administration, funding acquisition, and conceptualization.

Conflicts of interest

The authors declare that they have no known competing financial interests or personal relationships that could have appeared to influence the work reported in this paper.

Data availability

The data supporting this article are available in the main text and supplementary information (SI). The supplementary information contains raw NMR spectra of LA, SA, poly-LA hydrogel, and poly-LA-SA hydrogel, along with EDX spectra and surface elemental composition analyses of LA-G and LAS-G hydrogels. It also includes macroscopic wound images of the Control, Standard, LA-G, and LAS-G groups following wound induction. See DOI: https://doi.org/10.1039/d6ma00175k.

Acknowledgements

The authors are grateful to the Director CSIR-IHBT, Palampur, for providing the necessary facilities. A.S. acknowledges the financial assistance provided by CSIR under project MLP-204 and MLP002619 and the Department of Biotechnology GAP-0360 (File no. BT/NER/95/SP47015/2022). N.T. is grateful to the Department of Health Research (DHR), New Delhi, under grant reference No. R.11017/26/2023-GIA/HR. R. acknowledges CSIR, New Delhi, for the fellowship provided under File No. 31/054(0163)/2020-EMR-I. The authors would also like to acknowledge the Advanced Materials Research Center at the Indian Institute of Technology, Mandi, for carrying out PXRD and XPS analyses. Fig. 1, 6a and 7a were drawn using material provided by Servier Medical Art (https://www.smart.servier.com). During the preparation of this article, the author(s) used ''Grammarly'' to improve the language of the manuscript with appropriate caution. The author(s) reviewed and edited the content after using this tool and take full responsibility for the final version of the published article. The manuscript bears Institute communication no. 6073.

References

1 O. A. Peña and P. Martin, *Nat. Rev. Mol. Cell Biol.*, 2024, **25**, 599–616.
2 C. Chen, X. Yang, S.-J. Li, C. Zhang, Y.-N. Ma, Y.-X. Ma, P. Gao, S.-Z. Gao and X.-J. Huang, *Green Chem.*, 2021, **23**, 1794–1804.
3 W. Zhang, R. Wang, Z. Sun, X. Zhu, Q. Zhao, T. Zhang, A. Cholewinski, F. Yang, B. Zhao, R. Pinnaratip, P. K. Forooshani and B. P. Lee, *Chem. Soc. Rev.*, 2020, **49**, 433–464.
4 C. Liu, R. Lu, M. Jia, X. Xiao, Y. Chen, P. Li and S. Zhang, *Chem. Mater.*, 2023, **35**, 2588–2599.
5 S. Ahmad, M. Ahmad, K. Manzoor, R. Purwar and S. Ikram, *Int. J. Biol. Macromol.*, 2019, **136**, 870–890.
6 J. I. Kang and K. M. Park, *J. Mater. Chem. B*, 2021, **9**, 1503–1520.
7 P. Yang, Z. Li, B. Fang and L. Liu, *Int. J. Biol. Macromol.*, 2023, **253**, 127612.
8 R. Lei, M. Gu, J. Li, W. Wang, Q. Yu, R. Ali, J. Pang, M. Zhai, Y. Wang, K. Zhang, J. Yin and J. Xu, *Chem. Eng. J.*, 2024, **489**, 151499.
9 C. Zhao, E. Liu, F. Zhao, T. Wu, Q. Han, Z. Wang, R. Wang and J. Xing, *Int. J. Biol. Macromol.*, 2025, **331**, 148431.
10 Z. Zhang, Y. Wang, C. Wang, F. Yu, Y. Yuan and Z. Zhao, *J. Appl. Polym. Sci.*, 2025, **142**, e57021.
11 I. O. Levkovskyi, S. Mochizuki, A. Zheng, X. Zhang and F. Zhang, *Nano TransMed*, 2023, **2**, 100006.
12 Q. Yu, Z. Fang, S. Luan, L. Wang and H. Shi, *J. Mater. Chem. B*, 2024, **12**, 4574–4583.
13 J. Feng, W. Gao, P. Ge, S. Chang, T. Wang, Q. Zhao, B. He and S. Pan, *ACS Appl. Mater. Interfaces*, 2024, **16**, 65877–65889.
14 Q. Zhang, C.-Y. Shi, D.-H. Qu, Y.-T. Long, B. L. Feringa and H. Tian, *Sci. Adv.*, 2018, **4**, eaat8192.
15 C. Srinivasulu, M. Ramgopal, G. Ramanjaneyulu, C. Anuradha and C. S. Kumar, *Biomed. Pharmacother.*, 2018, **108**, 547–557.
16 A. Zochedh, M. Priya, C. Chakaravarthy, A. B. Sultan and T. Kathiresan, *Polycyclic Aromat. Compd.*, 2023, **43**, 6516–6548.
17 J. Ren, M. Yang, F. Xu, J. Chen and S. Ma, *Life Sci.*, 2019, **233**, 116728.
18 Y. Gao, X. Zhan, S. Huo, L. Fu, Z. Tang, K. Qi, C. Lv, C. Liu, Y. Zhu and S. Ding, *J. Mater. Chem. B*, 2022, **10**, 2171–2182.
19 Z. Liu, N. Shen, Z. Tang, D. Zhang, L. Ma, C. Yang and X. Chen, *Biomater. Sci.*, 2019, **7**, 2803–2811.
20 H. Patel, R. Singh and B. Datta, *RSC Adv.*, 2025, **15**, 29462–29478.
21 X. Hu, Q. Kong, R. Li, C. Zhou and Z. Li, *Fibers Polym.*, 2023, **24**, 3373–3384.
22 N. Khan and A. Saneja, *J. Mol. Struct.*, 2025, **1341**, 142652.
23 Y. Yang, G. He, Z. Pan, K. Zhang, Y. Xian, Z. Zhu, Y. Hong, C. Zhang and D. Wu, *Adv. Mater.*, 2024, **36**, 2404811.
24 A. K. Rana, R. Kumar, D. N. Shukla and D. Singh, *Free Radical Biol. Med.*, 2023, **207**, 107–119.
25 P. L. Bigliardi, S. A. L. Alsagoff, H. Y. El-Kafrawi, J.-K. Pyon, C. T. C. Wa and M. A. Villa, *Int. J. Surg.*, 2017, **44**, 260–268.
26 R. Singla, S. Soni, V. Patial, P. M. Kulurkar, A. Kumari, S. Mahesh, Y. S. Padwad and S. K. Yadav, *Int. J. Biol. Macromol.*, 2017, **105**, 45–55.
27 D. André-Lévigne, A. Modarressi, R. Pignel, M.-L. Bochaton-Piallat and B. Pittet-Cuénod, *Wound Repair Regen.*, 2016, **24**, 954–965.

28 H. Fang, T. Wang, Y. Zhu, G. Li, J. Yin, H. Cui and K. Zhang, *Small*, 2025, **21**, 2505959.
29 Q. Lu, X. Tang, K. Huang, S. Hu, B. Tao, W. Geng, Y. Lei, A. Guo and K. Li, *Mater. Today Bio*, 2025, **35**, 102504.
30 G. Stojkov, Z. Niyazov, F. Picchioni and R. K. Bose, *Gels*, 2021, **7**, 255.
31 L. Wang, G. Fan, L. Zhu, Y. Zhang, X. Wang, J. Qin, K. Lu, J. Hu and J. Ma, *J. Sci.:Adv. Mater. Devices*, 2024, **9**, 100677.
32 Ruchika, S. Kumari, P. Dhiman, D. Singh and A. Saneja, *J. Agric. Food Chem.*, 2022, **70**, 7674–7682.
33 A. Ntemafack, A. Qayum, S. K. Dhiman, M.-G. F. Guefack, S. Thapa, B. E. N. Wamba, V. Kuete, S. K. Singh, S. B. Bharate, Q. P. Hassan and S. G. Gandhi, *Curr. Microbiol.*, 2022, **80**, 7.
34 L. Han, X.-W. Liu, T. Zang, H. Ren, D.-S. Liang, S.-C. Bai, C. Li, X.-P. Liao, Y.-H. Liu and C. Zhang, *J. Controlled Release*, 2022, **351**, 896–906.
35 Ruchika, N. Thakur, N. V. Tirpude and A. Saneja, *Colloids Surf., B*, 2025, **254**, 114836.
36 S. Jha, A. Prabakaran, R. K. Sahoo, S. Batheja, U. Gupta and A. Alexander, *J. Drug Delivery Sci. Technol.*, 2024, **98**, 105902.
37 Z. Li, Z. Zhang, X. Ji, W. Wang, M. Xu, H. Cui, C. Du and L. Wang, *Chem. Eng. J.*, 2025, **512**, 162309.
38 R. G. Frykberg and J. Banks, *Adv. Wound Care*, 2015, **4**, 560–582.
39 Z. Xu, B. Liang, J. Tian and J. Wu, *Biomater. Sci.*, 2021, **9**, 4388–4409.
40 R. T. Polez, M. A. Ajiboye, M. Österberg and M. M. Horn, *Int. J. Biol. Macromol.*, 2024, **265**, 130808.
41 Z. Zhao, Q. Yang, Y. Sun and X. Ruan, *Front. Pharmacol.*, 2025, **16**, 1615294.
42 H. Liu, R. Ai, B. Liu and L. He, *Biomacromolecules*, 2025, **26**, 1541–1554.
43 A. Kumar, D. Kumar, K. Kumari, Z. Mkhize, L. M. K. Seru, I. Bahadur and P. Singh, *J. Mol. Liq.*, 2021, **322**, 114872.